

PAPER

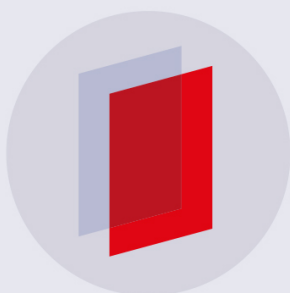
Arrays of electrically-addressable, optically-transmitting 3D nanostructures on free-standing, flexible polymer films

To cite this article: L A D'Imperio *et al* 2018 *Flex. Print. Electron.* **3** 025007

View the [article online](#) for updates and enhancements.

Related content

- [Optimization of the batch production of silicon fiber-top MEMS devices](#)
J H Rector, M Slaman, R Verdoold *et al.*
- [Fabrication of high aspect ratio tungsten nanostructures on ultrathin c-Si membranes for extreme UV applications](#)
F Delachat, B Le Drogoff, C Constanancias *et al.*
- [Engineering metallic nanostructures for plasmonics and nanophotonics](#)
Nathan C Lindquist, Prashant Nagpal, Kevin M McPeak *et al.*



IOP | ebooks™

Bringing you innovative digital publishing with leading voices to create your essential collection of books in STEM research.

Start exploring the collection - download the first chapter of every title for free.

Flexible and Printed Electronics



PAPER

Arrays of electrically-addressable, optically-transmitting 3D nanostructures on free-standing, flexible polymer films

L A D'Imperio , A F McCrossan, J R Naughton, J M Merlo, Y M Calm , M J Burns  and M J Naughton

Department of Physics, Boston College, 140 Commonwealth Avenue, Chestnut Hill, MA 02467, United States of America

E-mail: dimperil@bc.edu

Keywords: free-standing, flexible, nanocoax, photolithography, release layer, decapitation

RECEIVED
9 February 2018

REVISED
26 April 2018

ACCEPTED FOR PUBLICATION
31 May 2018

PUBLISHED
26 June 2018

Abstract

We describe the fabrication and properties of arrays of optically-transmitting 3D nanocylinders and nanocoaxes on free-standing, flexible, thin films made from a negative photoresist. The fabrication includes mostly standard lithographic techniques, enabled by the use of a release layer that allows separation of the thin film from the substrate in a simple final step. The chemical and mechanical stability of the polymer film and release layer enabled us to produce microstructures by multilayer photolithography as well as subsequent deposition of metal–insulator–metal layers to yield nanoscale coaxial pillars. We demonstrate the robust and flexible qualities of samples in interest of possible uses in wearable electronics and opto-bioelectronic interfacing.

Abbreviations

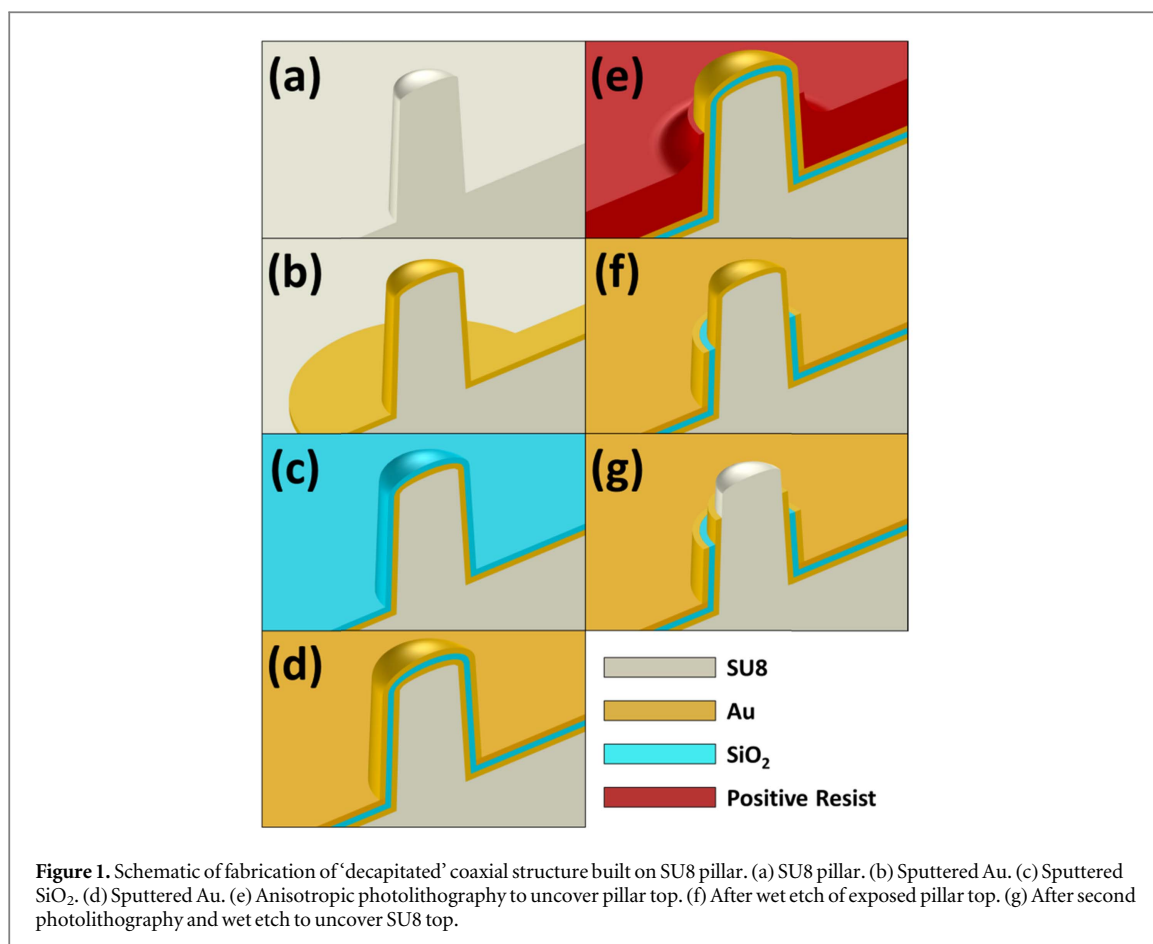
MEMS	Microelectromechanical systems
SEM	Scanning electron microscope
CMOS	Complementary metal–oxide–semiconductor
LED	Light-emitting diode

Introduction

Motivations for improving techniques and devices on flexible polymer thin films are numerous in areas such as wearable electronics, biomedical sensing, photonics, and MEMS [1–5]. In some instances the flexible films serve solely as a base in order to give substrate-based structures and devices access to applications and advantages of free-standing platforms. In other instances the aspects of the film are integral to the device function or process, e.g. the optically transparent and biocompatible properties of a film for optogenetic applications [6–9]. Many films are based on negative tone photoresists, due these materials' well known ability to be structured at the microscale [5, 10–12]. As application areas continue to expand, so do the requirements for the

stability and compatibility of free-standing films with a range of processes. In addition to the microstructuring of the polymer itself, the fabrication of many types of devices requires subsequent addition and modification of multiple layers. Previously reported materials, such as water-soluble germanium oxide [10] or common release layer materials, such as OmniCoat [13], are incapable of surviving such multistep processing. Aluminum oxide, Al_2O_3 , on the other hand, is a stable release layer material suitable for processing and eventual chemical release from a Si substrate.

This report presents a process yielding micro/nanopillar structures that require multilayer photolithography of a polymer resist as well as a multilayer process of electrical devices on a microstructured polymer. We were able to produce structures of interest that previously required a permanent substrate for fabrication [14]. In doing so, we demonstrate a process capable of providing current rigid substrate-based structures access to applications and advantages of free-standing platforms. As an example, this work focuses on the fabrication of vertical nanogap coaxial electrodes produced on polymer micropillar arrays on free-standing polymer films, toward potential applications in e.g. bioelectric and neuroelectric signal recording from devices, including the integration of local light delivery through the polymer-filled cores of



the pillars, however the technique reported here is not limited to these structures.

Methods

We divide the fabrication into three sections: thin flexible membrane, 3D microstructures on top of the membrane, and membrane release. While all sections are used in the fabrication of the samples described herein, it is important to note that these processes are independent of each other. More specifically, one could produce the 3D microstructures on a variety of substrates or perform the free-standing/release process for a range of structures or different material films.

Fabrication began with the deposition of a 150 nm thick layer of Al₂O₃ onto a Si wafer by atomic layer deposition, to act as a release layer. An 8.6 μm thick film of negative tone photoresist SU8-3010 (MicroChem) was spun onto the wafer, and standard process photolithography and baking was employed to produce eight separate 14 × 28 mm² thin film base regions. The same process parameters used for the base layer were used for the fabrication of the micro/nanostructures with the following exceptions: the resist used was SU8-2005 and a Cr photomask was employed which contained a 6 × 6 square array of 2 μm diameter circular holes with 30 μm pitch.

Polymerized SU8 resist underneath the holes yielded vertically-oriented pillars upon development.

The next part of the fabrication yielded nanogap coaxial metal–insulator–metal electrodes on the 6 × 6 array of SU8. The process for fabricating open-ended coaxial structures on the SU8 pillars is shown in the schematic in figure 1. Panel (a) shows a tilted, cross-sectional view of an SU8 pillar. Steps (b)–(d) include the sputter deposition of photolithographically-defined metal–insulator–metal layers. Steps (e)–(g) include the 'decapitation' of the coaxial pillar tops by a novel photolithographic process. The deposition of each material was performed by lift-off processing and sputter deposition. The layers depicted in steps (b), (c), and (d) are, respectively, 100 nm Au with 10 nm Ti above and below for increased adhesion, 150 nm SiO₂, and lastly, another 100 nm of Au preceded by 10 nm Ti. The first Au layer also defined individual electric address lines to each pillar in the 6 × 6 array, while the second Au layer formed a common electrical ground for all 36 pillars.

Steps (e)–(g) of figure 1 entail the uncovering of the topmost part of the coaxial pillars and then wet etching to remove the material from the pillar tops, in order to make the coax cores available for delivery of light from below. To do so, a layer of S1813 (MicroChem) was spin coated such that the resist thickness would be slightly less than the pillars' heights. The resist was exposed in flood exposure mode with a dose

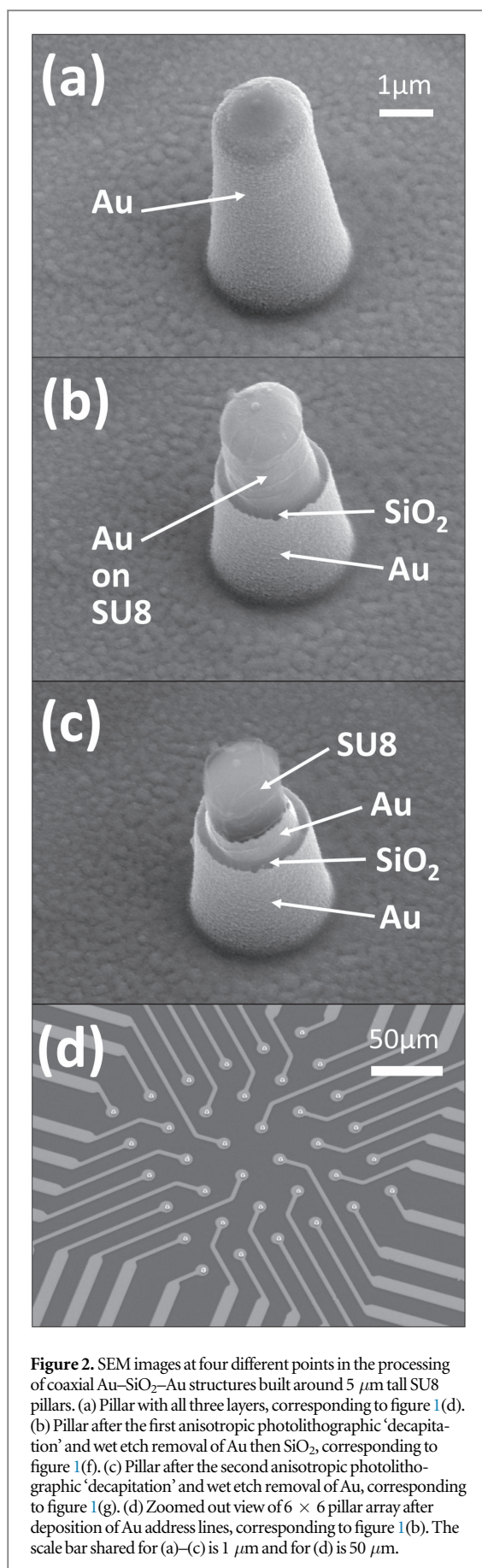


Figure 2. SEM images at four different points in the processing of coaxial Au-SiO₂-Au structures built around 5 μm tall SU8 pillars. (a) Pillar with all three layers, corresponding to figure 1(d). (b) Pillar after the first anisotropic photolithographic 'decapitation' and wet etch removal of Au then SiO₂, corresponding to figure 1(f). (c) Pillar after the second anisotropic photolithographic 'decapitation' and wet etch removal of Au, corresponding to figure 1(g). (d) Zoomed out view of 6 × 6 pillar array after deposition of Au address lines, corresponding to figure 1(b). The scale bar shared for (a)–(c) is 1 μm and for (d) is 50 μm.

that was much less than would be needed to expose the entire film thickness. During development, the majority of the resist remained undeveloped because

photo-acid generation occurs only in the topmost layer of the resist due to the low energy dose. The very thin resist that covered the topmost parts of the pillars was thus developed and removed, uncovering only the pillar top as shown in figure 1(e). Subsequent chemical wet etching was then used to remove Ti, Au and SiO₂ yielding the structure shown in figure 1(f). Another photo-decapitation was performed and another wet etch yielded the structure shown in figure 1(g). Finally, the wafer was submerged in MF-26A (MicroChem) for 24 h to release the thin SU8 films on which the microstructures reside. Tetramethylammonium hydroxide is the active developing component contained in MF-26A and is also responsible for contributing hydroxide ions to etch the alumina release layer [15]. The thin film samples were then removed from the solution, rinsed with alcohol and dried with N₂.

Results

Figures 2(a)–(c) show SEM images of a 5 μm tall pillar at points displayed in figure 1(e)–(g), respectively. Figure 2(d) shows a zoomed out SEM image of the individually electrically addressed pillars at the point displayed in figure 1(b) in order to emphasize the mesoscopic features.

The fabrication took place on a 100 mm diameter Si wafer where eight samples were simultaneously processed, each of which ultimately contained a 6 × 6 array of coaxial SU8 pillars. Inspection by an optical microscope and SEM showed 100% yield in lithographic pillar formation for the 288 pillars from the process described herein. The individually addressed pillars are shown in the optical microscope image of figure 3(a) as small dark spots at the end of each address line. After the remaining process steps, ending with the release of the film, the free-standing sample was set onto a glass slide and imaged from above the pillar array, while back-side illumination allowed observation of the transmitted light localized through the tops of the pillars, as seen in the figure 3(b) bright-field image.

This feature can enable application of these films in microelectrode array devices with optical access. For example, one could integrate optical stimulation of electrogenic cells simultaneous to electrical recording by the coax inner electrode, similar to that recently demonstrated in rigid (nonflexible) coaxial structures [14].

A key component of the fabrication of these samples was the ability of the SU8 to remain well-secured to the wafer through multiple steps and in chemically harsh conditions, e.g., heated 1165 and acid etchants, yet later be removable from the substrate. The Al₂O₃ film is very robust in this regard and there was no unintentional delamination at any point in the fabrication. This enabled multistep fabrication that would

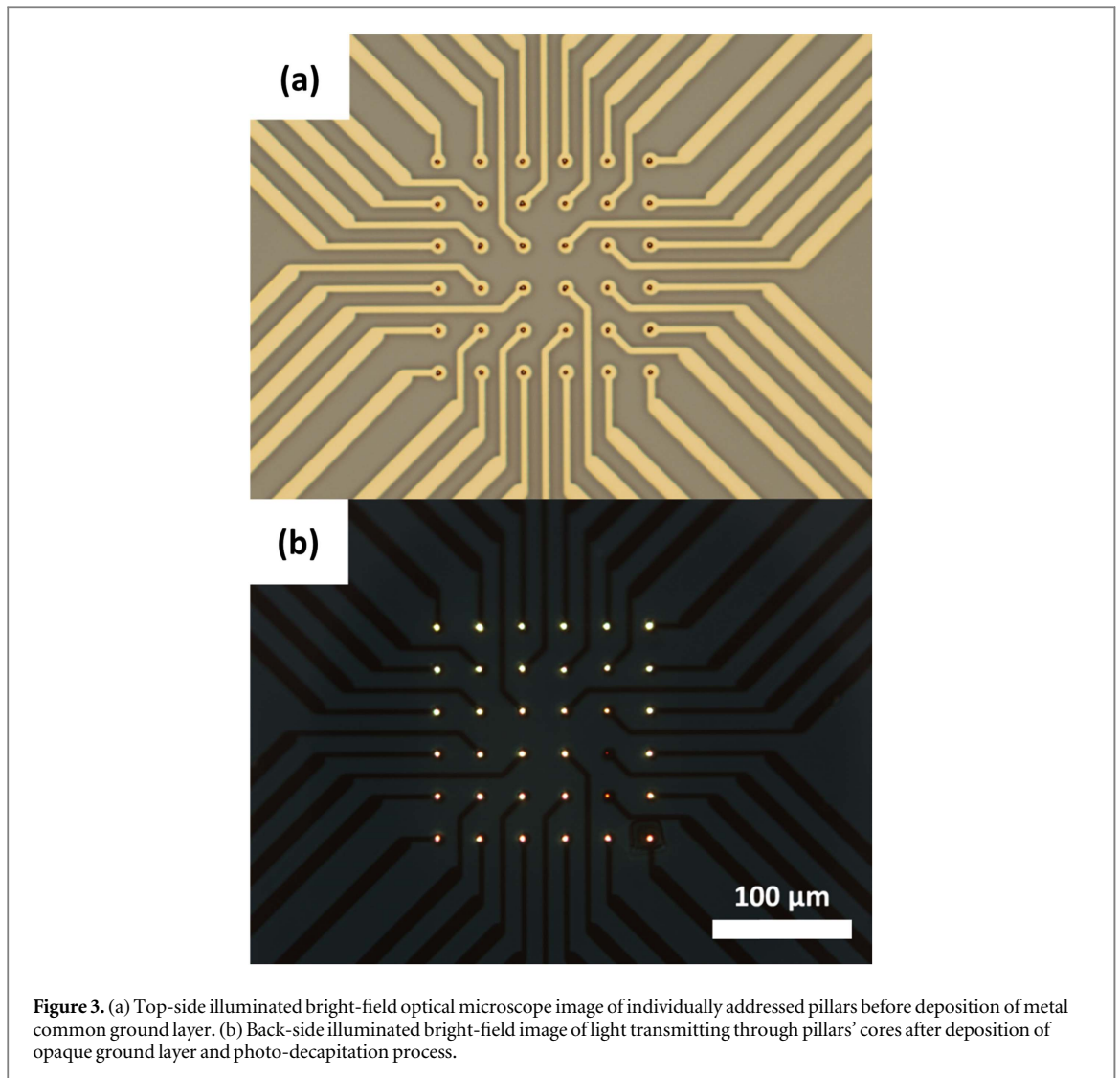


Figure 3. (a) Top-side illuminated bright-field optical microscope image of individually addressed pillars before deposition of metal common ground layer. (b) Back-side illuminated bright-field image of light transmitting through pillars' cores after deposition of opaque ground layer and photo-decapitation process.

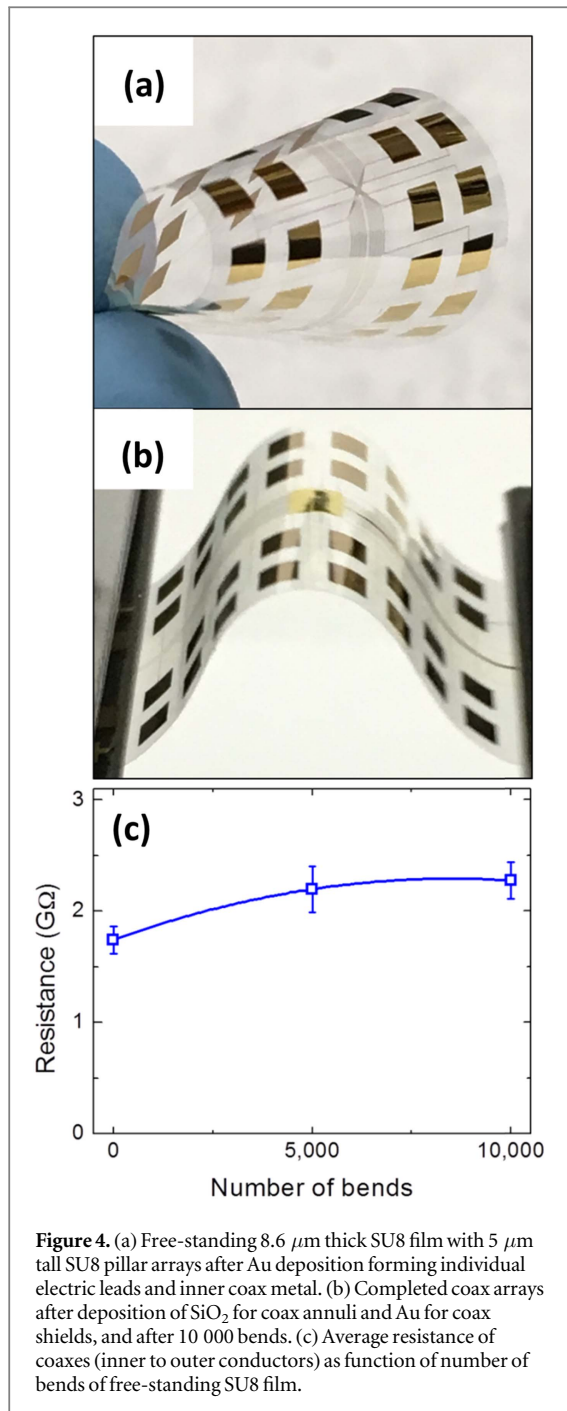
not be possible with other easily dissolvable release materials [10, 13]. We note also that the MF-26A release solution used above is CMOS-compatible.

The SU8 films were measured to be $8.6 \mu\text{m}$ thick (Dektak Profilometer), a value readily varied by adjusting the SU8 viscosity and spin speed (we have made films with controlled thicknesses from 3 to $30 \mu\text{m}$). Once released, these SU8 films showed good durability to handling and testing. Figure 4 includes pictures of free-standing samples: figure 4(a) shows a sample bent between two fingers that was released after the deposition of the first Au layer that defines the square contact pads, electric leads, and inner coaxial metal, while figure 4(b) shows a final sample after the entire process with all layers.

As a way of further testing the robustness of the SU8 films and integrated microstructures, the resistance of each individual coaxial structure was measured (Keithley 6512 Electrometer) before and after numerous 180° bendings controlled by a DM542 digital stepper drive [16]. Given that large changes in the $G\Omega$ resistances would indicate shorting or disconnecting, we are able to use this measurement to determine

whether the microstructures or the Au microwires experience damage due to repeated bending. A bending radius of 2.5 mm was used in this bending test. Additional static bending tests were performed in order to confirm that smaller bending radii down to $150 \mu\text{m}$ were achievable before the SU8 films would start experiencing deformation. Figure 4(c) shows the average resistance of the coaxes after 0, 5000 and 10 000 bends. After 10 000 bends, the yield of viable coaxes was $\sim 80\%$, with viable defined as a coax having resistance less than five standard deviations from the original mean value. Coaxes with resistance outside of this range were likely either shorted by some part of the inner and outer metals touching, or open circuit by a break in a lead. There were no observable changes to the macroscopic characteristics of the film before and after bend tests. In fact, the photo of the sample in figure 4(b) was taken after the 10 000 bend test.

Free-standing SU8 films with larger ($\sim 10 \text{ cm}^2$) regions of SU8 pillars were also fabricated to test potential for scaling to larger arrays ($\sim 10^6$ pillars). Both photolithography and nanoimprint lithography were capable of producing such arrays with nearly 100% yield in pillar



formation, similar to our previously reported work on Si substrates [17]. Free-standing SU8 films with larger bases were also fabricated to test the capability of wafer-scale thin films. Thin films were easily achieved for all sizes attempted (up to 80 mm diameter). Lastly, similar free-standing samples were also produced using H.A.R.E SQ (KemLab Inc.), a negative photoresist similar to SU8.

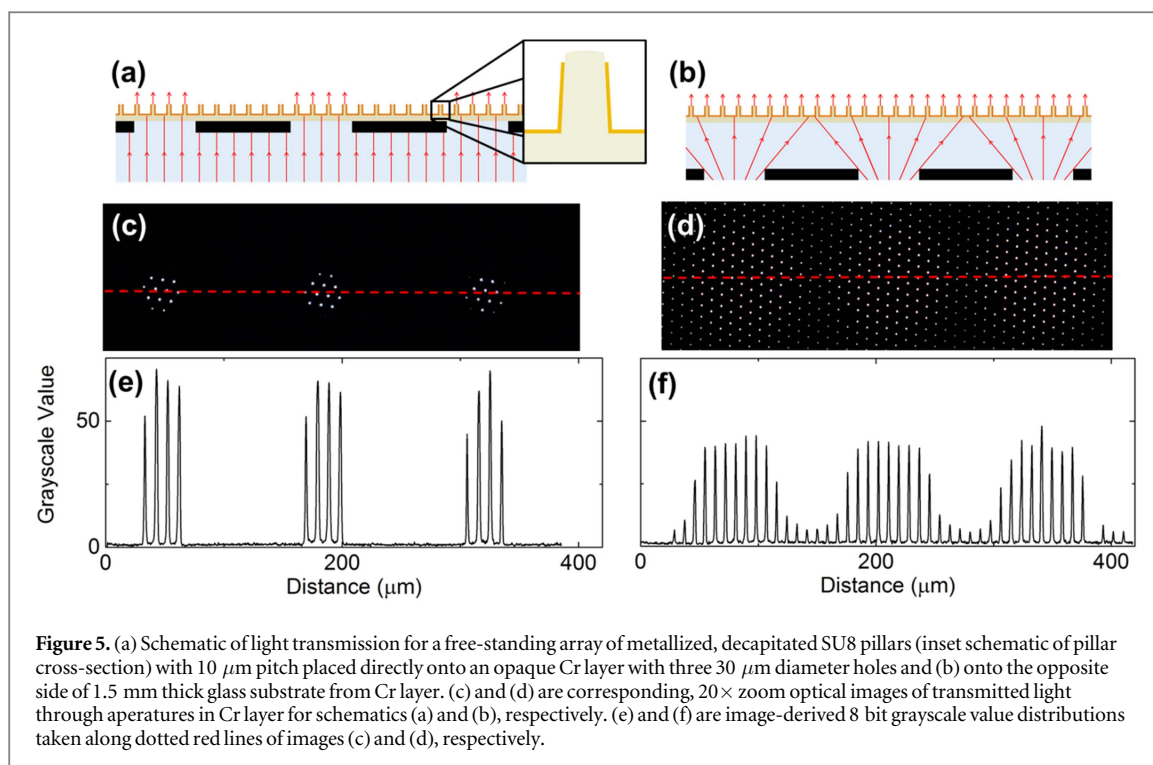
Discussion

While materials like phospho-silicate-glass are commonly used as sacrificial layers in MEMS fabrication,

criteria for a material to be used as a sacrificial layer are that it be mechanically robust, have sufficient adhesion to the materials within which it will be embedded, be reasonably thermally matched to these materials, and be amenable to etching processes that are highly selective towards it compared to the other materials in the structure at the time it needs to be removed. In specialized cases, there may be additional criteria such as epitaxial matching [18]. Aluminum oxide is a good choice for a release layer in our structure due to a combination of considerations. Alumina is a readily available and inexpensive material that can be produced as a thin film by different standard methods, such as by physical vapor deposition, atomic layer deposition and anodization of aluminum. Alumina also has a relatively high thermal conductivity, e.g., an order of magnitude higher than that of SiO_2 for the range of processing temperatures used. In our case, we believe this is important for the heat transfer into the SU8 films during different baking steps. SU8 films demonstrated increased adhesion to alumina surfaces compared with SiO_2 surfaces throughout the varying chemical and physical conditions of the fabrication process. The alumina layer is robust to most gaseous chemicals and therefore is capable of withstanding oxygen microwave barrel etching used for surface cleaning and SU8 adhesion promotion steps. The TMAH responsible for etching the alumina does not affect the SU8, Au, Ti or SiO_2 that are to remain in the final structure. Altogether, the alumina layer is a well-matched, chemically and physically robust material during all process steps except for the final step of removal, where its etchant is highly selective to it against the other materials in the structure.

The deposition rate of alumina depends on the process and parameters used for that process. The deposition by ALD of alumina for samples described in this work occurs at 3.75 nm min^{-1} . The cycle time almost entirely consists of the 8 s wait times after the 15 ms pulses of $(\text{CH}_3)_3\text{Al}$ (trimethylaluminum) and H_2O . There are many factors that can specifically affect this rate, e.g., chamber size, pump rate, substrate/chamber temperature, addition of ozone or plasmas, pulse length, and different deposition schemes achieving rates of 30 nm min^{-1} for ALD [19]. Additionally, alumina thicknesses other than the 150 nm used in this study are suitable as a release layer, though a systematic study as such was not performed. An alumina thickness of 150 nm was used to release a 75 mm diameter circular SU8 film, thereby demonstrating that this thickness could be used for any wafer-scale SU8 film release applications. The deposition rate of alumina by other processes, such as sputtering or thermal deposition, vary widely and can achieve rates up to 500 nm min^{-1} [20].

The etch rate of an exposed surface of ALD alumina in MF-26A was measured to be 3.5 nm min^{-1} . However, underneath the SU8 films the etch rate, as



determined by the 24 h release time of a $14\ \text{mm}$ -wide film, is drastically accelerated, possibly by capillary forces in the small gap and inherent stresses that remain at SU8-alumina interface. (The expected etching time @ $3.5\ \text{nm}\ \text{min}^{-1}$ for $14\ \text{mm}$ would be three orders of magnitude larger.) While a systematic study of the alumina thickness versus release time was not performed, it is plausible that a decrease or increase in alumina layer thickness would decrease the release time. Other possible methods for decreasing the etch time include stirring the samples during release, using a solution with higher concentration TMAH, and increasing the solution temperature. One would want to make sure that large process changes would not affect materials or structures of the sample.

Potential applications of the design presented herein include interfacing with micro-LED arrays for e.g. bioelectronics. That is, the small substrate thickness can enable one-to-one correlation of LEDs and optically-transmitting coaxial pillars that would not be possible with thicker substrates or with the thick ($>100\ \mu\text{m}$) coverglasses of current pixel displays. Such localization and diffraction of a light source for the current device is demonstrated in figure 5.

There, a $5\ \mu\text{m}$ thick, free-standing film with $\sim 10^6$ metallized, decapitated pillars was placed in direct contact with an opaque Cr film (on $1.5\ \text{mm}$ thick glass) containing an array of $30\ \mu\text{m}$ diameter holes at $150\ \mu\text{m}$ pitch. In this case, light is only able to pass through the pillars that are directly above the holes in the Cr, figure 5(c). In figure 5(d), separating the Cr holes from the pillar array by the $1.5\ \text{mm}$ thick substrate causes considerable diffraction on length scales greater than the pillar pitch, preventing one-to-one

light source-to-pillar transmittance. Figure 5(e) and (f) are the corresponding light intensity distributions along the dashed red lines superimposed in figures 5(c) and (d), respectively. Through one-to-one correlation of coaxial pillars with micro-LEDs, one could simultaneously achieve localization of optical stimulation with localization of electrical recording [14] in an opto-bioelectronic interface.

Conclusion

In summary, we described the fabrication and characterization of arrays of 3D nanocoaxial structures on thin, free-standing, and flexible polymer films made from negative photoresist. Al_2O_3 was shown to be a robust and easily-removable release layer material for the multiple processing steps. Similar robustness was exhibited in the thin films and micro/nanostructures as well as the photolithographically-defined metal-insulator-metal layers. Optical transmission of light through coax cores was demonstrated. Such free-standing arrays on flexible thin films with localized optical throughput and localized electrical recording could be useful tools for optically-integrated devices, for example for bioelectric and neuroelectronic measurements. The short optical path length afforded by such thin (sub- $10\ \mu\text{m}$ thick) films is instrumental in eliminating diffraction effects in e.g. μLED array integration for such uses, as light from a single LED pixel and passing through conventional, thick substrates would disperse across many coax pixels, rendering them inappropriate for localized light delivery.

Acknowledgment

The authors thank Steve Shepard in the Boston College Integrated Science Clean Room Facility for assistance in device fabrication.

Author contributions

The manuscript was written through contributions of all authors. All authors have given approval to the final version of the manuscript.

Notes

The authors declare no competing financial interest.

ORCID iDs

L A D'Imperio  <https://orcid.org/0000-0001-8281-2552>

Y M Calm  <https://orcid.org/0000-0002-6216-396X>

M J Burns  <https://orcid.org/0000-0001-9804-405X>

References

- [1] Xu L *et al* 2014 3D multifunctional integumentary membranes for spatiotemporal cardiac measurements and stimulation across the entire epicardium *Nat. Commun.* **5** 3329
- [2] Kenry Y J C and Lim C T 2016 Emerging flexible and wearable physical sensing platforms for healthcare and biomedical applications *Microsyst. Nanoeng.* **2** 16043
- [3] Qiao W, Huang W, Liu Y, Li X, Sen C L and Tang J X 2016 Toward scalable flexible nanomanufacturing for photonic structures and devices *Adv. Mater.* **28** 10353–80
- [4] Sim K, Rao Z, Li Y, Yang D and Yu C 2018 Curvy surface conformal ultra-thin transfer printed Si optoelectronic penetrating microprobe arrays *npj Flex. Electron.* **2** 2
- [5] Ornoff D M, Wang Y and Allbritton N L 2013 Characterization of freestanding photoresist films for biological and MEMS applications *J. Micromech. Microeng.* **23** 025009
- [6] Kwon K Y, Lee H-M, Ghovanloo M, Weber A and Li W 2015 Design, fabrication, and packaging of an integrated, wirelessly-powered optrode array for optogenetics application *Front. Syst. Neurosci.* **9** 69
- [7] Kuzum D *et al* 2014 Transparent and flexible low noise graphene electrodes for simultaneous electrophysiology and neuroimaging *Nat. Commun.* **5** 5259
- [8] Lee W, Kim D, Matsuhisa N, Nagase M, Sekino M, Malliaras G G, Yokota T and Someya T 2017 Transparent, conformable, active multielectrode array using organic electrochemical transistors *Proc. Natl Acad. Sci.* **114** 10554–9
- [9] Heo C, Park H, Kim Y T, Baeg E, Kim Y H, Kim S G and Suh M 2016 A soft, transparent, freely accessible cranial window for chronic imaging and electrophysiology *Sci. Rep.* **6** 27818
- [10] Ha B, Nam J and Jo S 2017 Releasable SU-8 structures for various microfabrication processes using a water-soluble sacrificial layer *Microelectron. Eng.* **172** 49–54
- [11] Sato H, Matsumura H, Keino S and Shoji S 2006 An all SU-8 microfluidic chip with built-in 3D fine microstructures *J. Micromech. Microeng.* **16** 2318–22
- [12] Aracil C, Perdignes F, Moreno J M and Quero J M 2010 BETTS: bonding, exposing and transferring technique in SU-8 for microsystems fabrication *J. Micromech. Microeng.* **20** 035008
- [13] MicroChemicals X P SU-8 Release Layer <http://microchem.com/pdf/OMNICOAT.pdf>
- [14] Naughton J R, Connolly T, Varela J A, Lundberg J, Burns M J, Chile T C, Christianson J P and Naughton M J 2016 Shielded coaxial optrode arrays for neurophysiology *Front. Neurosci.* **10** 252
- [15] Sun K G, Li Y V, Saint John D B and Jackson T N 2014 PH-controlled selective etching of Al₂O₃ over ZnO *ACS Appl. Mater. Interfaces* **6** 7028–31
- [16] Leadshine Technology Co 2012 User's manual for DM542 Fully Digital Stepper Drive http://leadshine.com/UploadFile/Down/DMSHm_P.pdf
- [17] Rizal B, Merlo J, Burns M, Chiles T and Naughton M J 2015 Nanocoaxes for optical and electronic devices *Analyst* **140** 39–58
- [18] Lee L P, Burns M J and Char K 1992 Free-standing microstructures of YBa₂Cu₃O_{7-δ}: a high-temperature superconducting air bridge *Appl. Phys. Lett.* **61** 2706–8
- [19] Werner F, Stals W, Görtzen R, Veith B, Brendel R and Schmidt J 2011 High-rate atomic layer deposition of Al₂O₃ for the surface passivation of Si solar cells *Energy Proc.* **8** 301–6
- [20] Jones F and Logan J 1989 High-rate reactive sputter deposition of aluminum oxide *J. Vac. Sci. Technol. A* **7** 1240–7